Numerical study of the effects of tsunamis using a finite element method

Y. Otani[1] K. Yamamoto[2] Hashentuya[3]
M. Watanabe[4]

(Received 31 January 2011; revised 5 November 2011)

Abstract

Effects of tsunamis generated in water areas surrounding Japan are studied numerically. Partial differential equations consisting of momentum equations and a continuity equation are reduced to a system of ordinary differential equations with discretisation based on a finite element mesh. An ordinary differential equation solver is applied to the resultant system to generate numerical solutions. Depth data formulated in terms of longitude and latitude in the horizontal direction are transformed to generate input data in terms of projected coordinates by the Gauss–Krüger projection. Numerical results are visualised, and effects of tsunamis such as wave heights and propagation speeds are illustrated. Numerical techniques to simulate tsunamis are described, and numerical results are introduced.

Contents

1 Introduction

About 10% of earthquakes occur in Japan. There are about ten tectonic plates on the earth and four of them accumulate around the islands of Japan [5]. Many tsunamis are caused by them. The wave height of the Okushiri Island Tsunami (1993) was over 30 m, while the run-up on the river of the Tokachi Oki Tsunami (2003) was over 11 km. For the prevention of disasters various techniques concerning forecasting or simulation of tsunamis are researched. The Nankai Trough is the area where the Philippine Sea plate meets the Eurasian plate and subducts under that. In this area large earthquakes have occurred periodically together with the Suruga Trough. The latest Nankai earthquake was in 1946. Preparedness for the next one is an urgent theme of disaster prevention in Japan. We simulated the 1946 Nankai earthquake by the finite element method based on the parameters of its fault displacements. The technique of mesh refinement according to the sea depth is also shown.

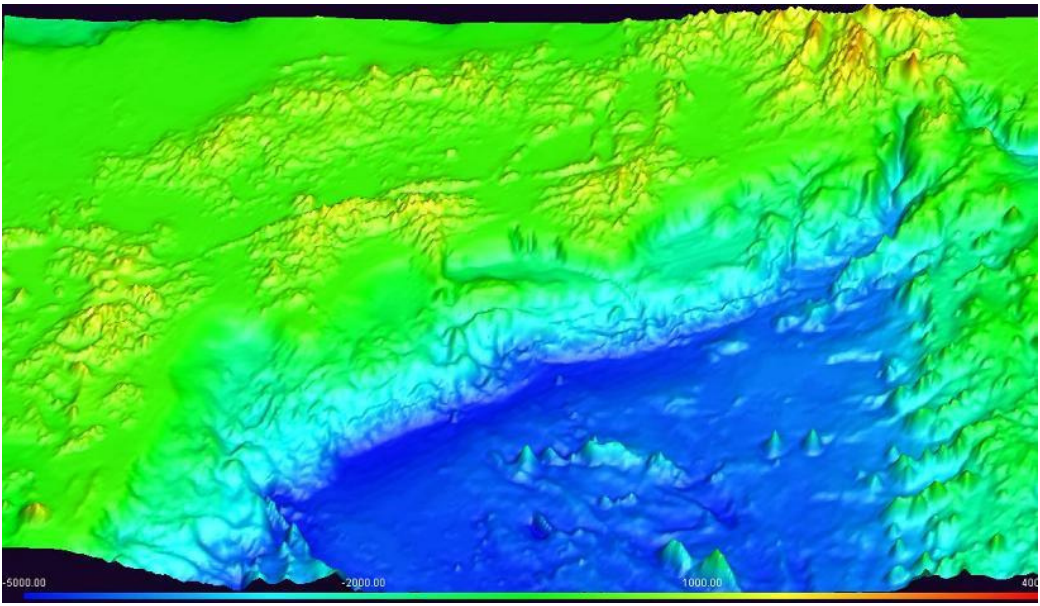

Figure 1: Nankai Trough.

The results are visualised and the behaviour of the wave in the shore and the shore offing are compared.

2 Mesh structure and refinement

The simulation area ranges from latitude 30° to 36° North and longitude 130° to 140° East; Figure 1 shows the topography of this area. The coordinates according to these latitude and longitude are converted to those of a rectangular coordinate system by the Gauss–Krüger projection. The structured elements shown in Figure 2 are set on this area.

The area is divided into two hundred and forty segments from south to north and divided into four hundred segments from east to west and rectangular

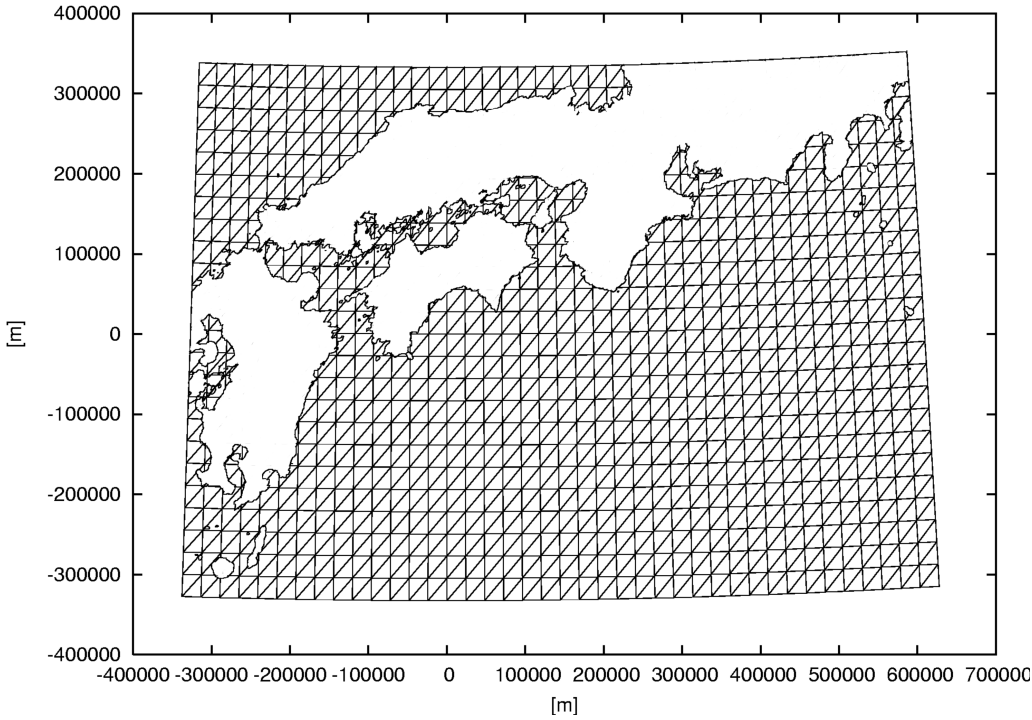

Figure 2: Image of elements.

grids are set. A triangular mesh is generated by dividing each rectangle into two triangles. The width of each element is approximately 2400 m and the height is approximately 2800 m. The wave length of a tsunami is long enough compared to the sizes of elements over a deep sea area. However, over a shallow water region the wave length becomes shorter and the sizes of elements are required to be smaller. The nonlinear terms become significant over a shallow water area, and we apply a nonlinear model different from the linear equations over a deep sea area as described in Section 4. The first refinement is applied to the elements over the area shallower than two hundred meters and the second refinement is applied to the elements over the area shallower than fifty meters. Techniques are based on two factors,

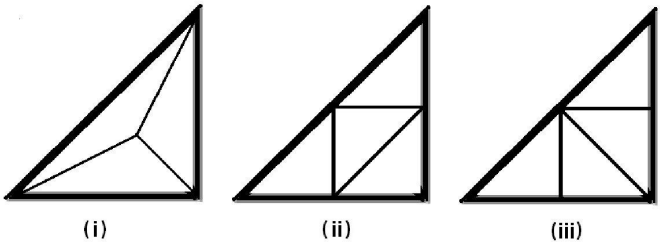

Figure 3: Mesh refinement methods.

keeping the shape of the triangles unchanged and minimising the influence of the division of one triangle to adjacent elements.

The way an element is subdivided affects not only the shapes of its child elements, but also the number of neighbouring elements that need to be subdivided. The method (i) in Figure 3 does not affect any other elements, but makes the element shapes inadequate. The method (ii) keeps the element shape, but affects neighbour elements endlessly, as shown in Figure 4(a). We adopt the remeshing method (iii). According to this division all influences are shown in Figure 4(b). At most five elements are affected by this division.

Our original coarse mesh is shown in Figure 5, and Figure 6 shows the refined meshes. After the last refinement the smallest element has almost 600 m width and 700 m length.

3 Initial condition

The initial sea surface deformation caused by a submarine earthquake is equal to the vertical displacement of the sea floor as long as the width of the fault is much longer than the sea depth. The displacement of the sea floor is calculated using the parameters of the earthquake [3]. The Nankai Earthquake in 1946 consisted of two large fault displacements.

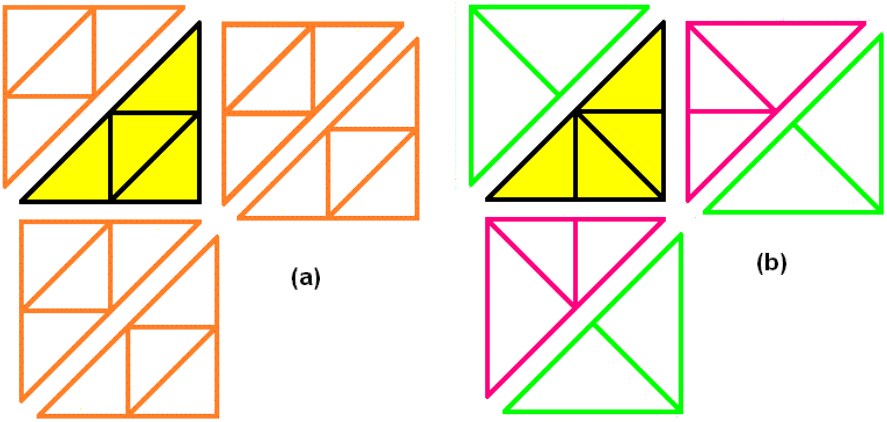

Figure 4: Influences of division.

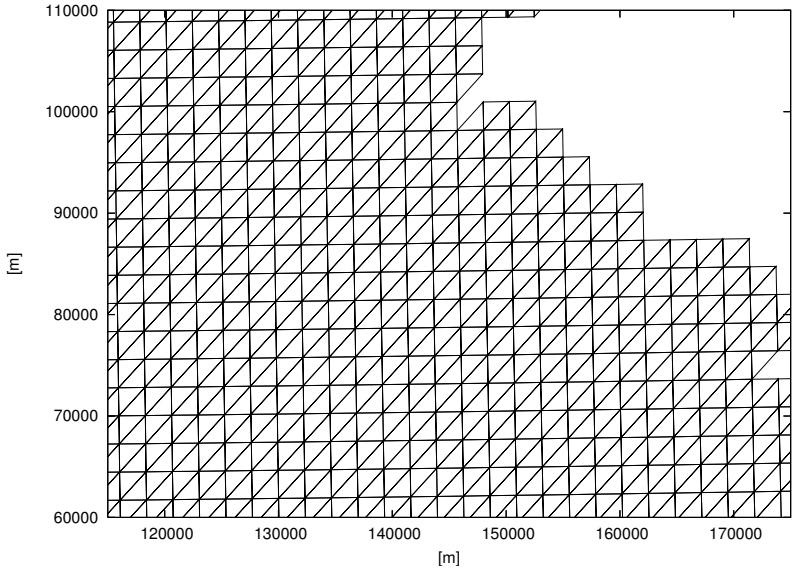

Figure 5: Original coarse mesh.

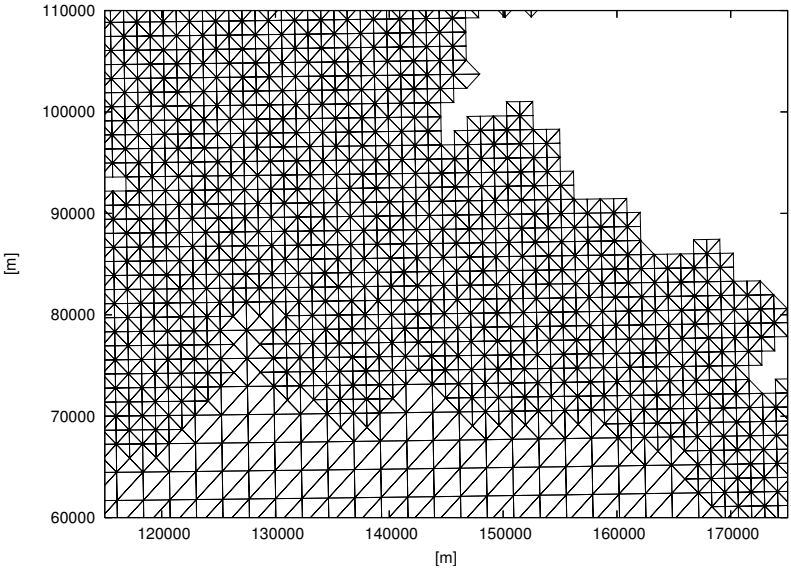

(a) First refinement.

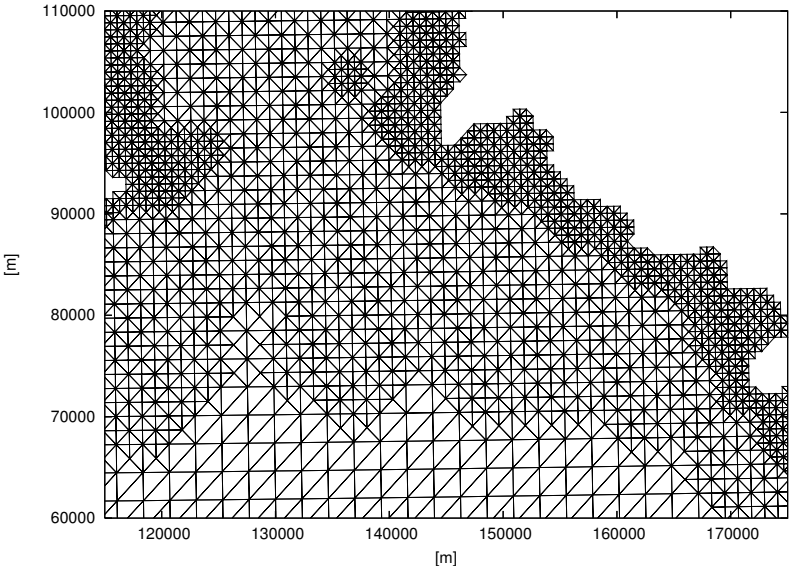

(b) Second refinement.

Figure 6: Result of mesh refinement.

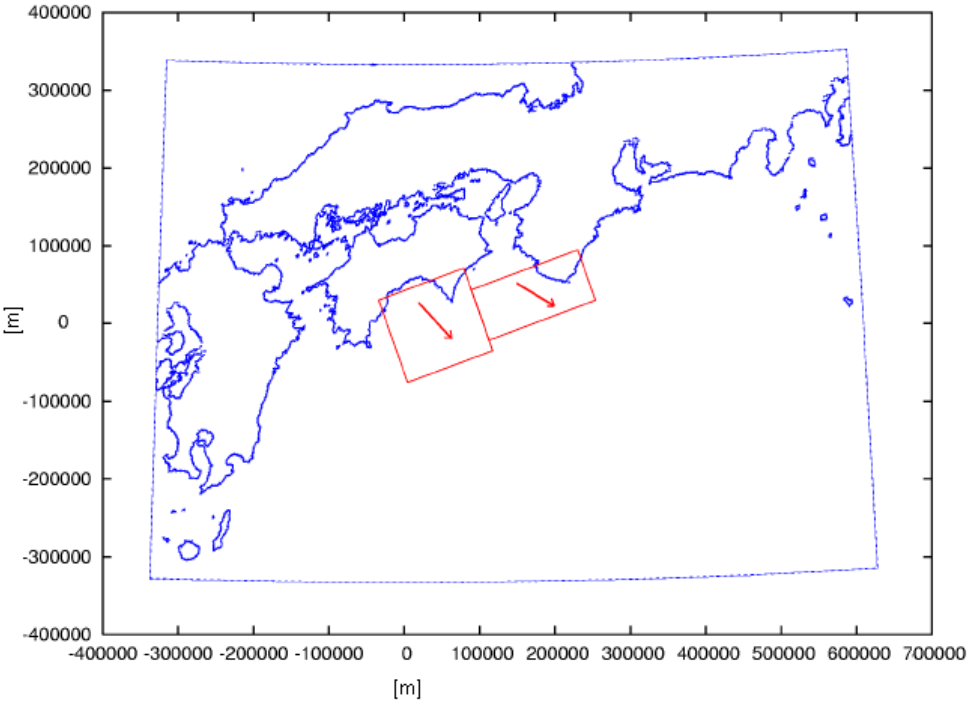

Figure 7: Fault map.

Table 1 lists the parameters of the two faults in the Nankai Earthquake of 1946 [1]: L is the length, W is the width, θ is the horizontal angle, λ is the slip angle, Z is the depth, δ is the dip angle, U is the slip amount, N is north latitude, and E is east longitude of the fault. Figure 7 shows the locations of those faults. The coordinate origin of Figure 7 is the origin of the Gauss–Krüger projection. Figure 8 shows the initial displacement of the sea surface, according to the parameters in Table 1.

Table 1: Fault parameters

part	L (km)	W (km)	θ (°)	λ (°)	Z (km)	δ (°)	U (cm)	N (°)	E (°)
East	150	70	250	127	10	20	400	33.24	136.22
West	120	120	250	104	1	10	500	32.68	134.75

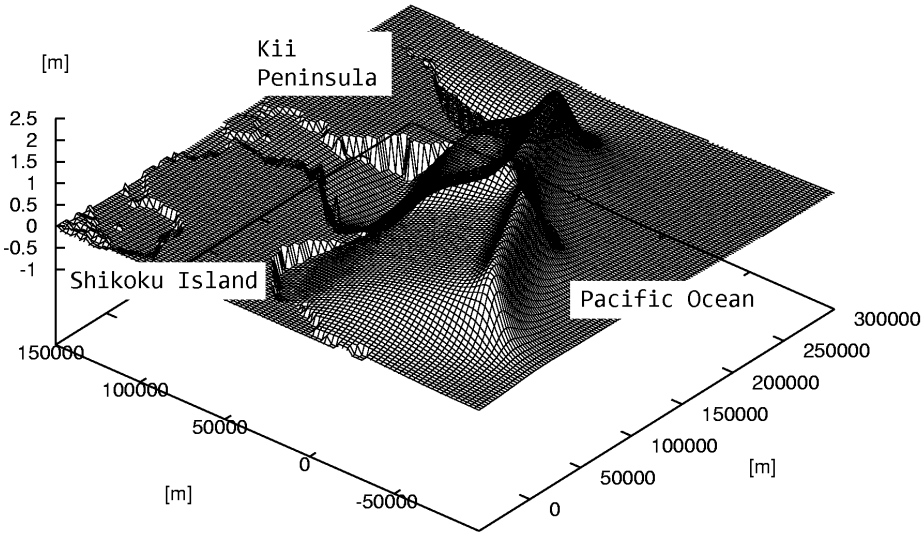

Figure 8: Result of integration (bird's eye view).

4 Governing equations

The system of partial differential equations consists of momentum equations and the continuity equation:

$$\frac{\partial M}{\partial t} + \frac{\partial}{\partial x}\left(\frac{M^2}{D}\right) + \frac{\partial}{\partial y}\left(\frac{MN}{D}\right) + gD\frac{\partial \zeta}{\partial x} + \frac{gn^2}{D^{7/3}} M\sqrt{M^2+N^2} = 0\,, \quad (1)$$

$$\frac{\partial N}{\partial t} + \frac{\partial}{\partial x}\left(\frac{MN}{D}\right) + \frac{\partial}{\partial y}\left(\frac{N^2}{D}\right) + gD\frac{\partial \zeta}{\partial y} + \frac{gn^2}{D^{7/3}} N\sqrt{M^2+N^2} = 0\,, \quad (2)$$

$$\frac{\partial \zeta}{\partial t} + \frac{\partial M}{\partial x} + \frac{\partial N}{\partial y} = 0\,. \quad (3)$$

Here, M and N are the x and y-components of the flux, defined by

$$M = \int_{-h}^{\zeta} u\, dz\,, \quad N = \int_{-h}^{\zeta} v\, dz\,,$$

where u and v represent the x-component and y-component of velocity respectively. The total depth is $D = h + \zeta$, where h is sea depth and ζ is water surface elevation. The constant g is gravitational acceleration and n is the Manning roughness coefficient. In the deep sea, where ζ is small enough in comparison to h, the nonlinear advection and bottom friction terms in (1) and (2) are negligible so the equations of momentum become linear

$$\frac{\partial M}{\partial t} + gD\frac{\partial \zeta}{\partial x} = 0\,, \quad (4)$$

$$\frac{\partial N}{\partial t} + gD\frac{\partial \zeta}{\partial y} = 0\,. \quad (5)$$

Most of the sea area is deep enough to apply linear theory. But the shallow water theory must be applied where the depth is shallower than 50 m.

5 Discretisation of the governing equations

This section presents only the numerical technique for the linear model over a deep sea area. For our FEM analysis, we let

$$\begin{aligned} M(x,y,t) &\approx \sum_{j=1}^{n} M_j(t)\Phi_j(x,y), \\ N(x,y,t) &\approx \sum_{j=1}^{n} N_j(t)\Phi_j(x,y), \\ \zeta(x,y,t) &\approx \sum_{j=1}^{n} \zeta_j(t)\Phi_j(x,y), \\ h(x,y) &\approx \sum_{j=1}^{n} h_j\Phi_j(x,y), \end{aligned} \tag{6}$$

where $\Phi_1, \Phi_2, \ldots, \Phi_n$ are piecewise linear basis functions which satisfy

$$\Phi_i(x_j, y_j) = \delta_{ij}\,, \quad i,j = 1,2,\ldots,n\,,$$

δ_{ij} is the Kronecker delta function, and n is the total number of nodes. The system of governing equations is

$$\begin{aligned} &\sum_{j=1}^{n} \frac{\partial M_j}{\partial t}\Phi_j + g\frac{\partial \zeta}{\partial x}\sum_{j=1}^{n}(h_j+\zeta_j)\Phi_j = 0\,, \\ &\sum_{j=1}^{n} \frac{\partial N_j}{\partial t}\Phi_j + g\frac{\partial \zeta}{\partial y}\sum_{j=1}^{n}(h_j+\zeta_j)\Phi_j = 0\,, \\ &\sum_{j=1}^{n} \frac{\partial \zeta_j}{\partial t}\Phi_j + \frac{\partial M}{\partial x} + \frac{\partial N}{\partial y} = 0\,. \end{aligned} \tag{7}$$

At every node (x_i, y_i) the system of equations (7) becomes

$$\frac{dM_i}{dt} = -g(h_i+\zeta_i)\frac{\partial \zeta}{\partial x}\,,$$

$$\frac{dN_i}{dt} = -g(h_i + \zeta_i)\frac{\partial \zeta}{\partial y},$$
$$\frac{d\zeta_i}{dt} = -\left(\frac{\partial M}{\partial x} + \frac{\partial N}{\partial y}\right). \tag{8}$$

Each partial derivative on the right-hand side of (8) is approximated by the average of the values of the partial derivative over the elements that have the node in common as one of their vertices [6]. The method of collocation [4] is implemented, and the partial derivative at the ith node is

$$\left(\frac{\partial \zeta}{\partial x}\right)_i = \frac{1}{\sum_{k=1}^{m} A_k} \sum_{k=1}^{m} A_k \left(\frac{\partial \zeta}{\partial x}\right)^{(k)} \tag{9}$$

where $A_1, A_2, \ldots A_m$ are the areas of the elements that have the ith node in common and $(\partial\zeta/\partial x)^{(k)}$ is an approximate value of the partial derivative $(\partial\zeta/\partial x)$ in the kth element.

The fourth order Adams–Bashforth–Moulton predictor-corrector method in PECE mode is used to solve the system of equations (9) numerically, together with the fourth order Runge–Kutta method, which is used to generate approximate solutions in the first three steps [2].

The discretisation shown in the system of equations (8) is similarly applied to the nonlinear equations (1)–(3) over a shallow water area as

$$\frac{dM_i}{dt} = -\frac{\partial}{\partial x}\left(\frac{M^2}{D}\right) - \frac{\partial}{\partial y}\left(\frac{MN}{D}\right) - gD_i\frac{\partial \zeta}{\partial x} - \frac{gn^2}{D_i^{7/3}} M_i \sqrt{M_i^2 + N_i^2},$$
$$\frac{dN_i}{dt} = -\frac{\partial}{\partial x}\left(\frac{MN}{D}\right) - \frac{\partial}{\partial y}\left(\frac{N^2}{D}\right) - gD_i\frac{\partial \zeta}{\partial y} - \frac{gn^2}{D_i^{7/3}} N_i \sqrt{M_i^2 + N_i^2},$$
$$\frac{d\zeta_i}{dt} = -\left(\frac{\partial M}{\partial x} + \frac{\partial N}{\partial y}\right), \tag{10}$$

where $D_i = h_i + \zeta_i$. The partial derivatives on the right-hand sides of the equations (10) become

$$\frac{\partial}{\partial x}\left(\frac{M^2}{D}\right) = 2\frac{M_i}{D_i}\frac{\partial M}{\partial x} - \frac{M_i^2}{D_i^2}\frac{\partial D}{\partial x} \tag{11}$$

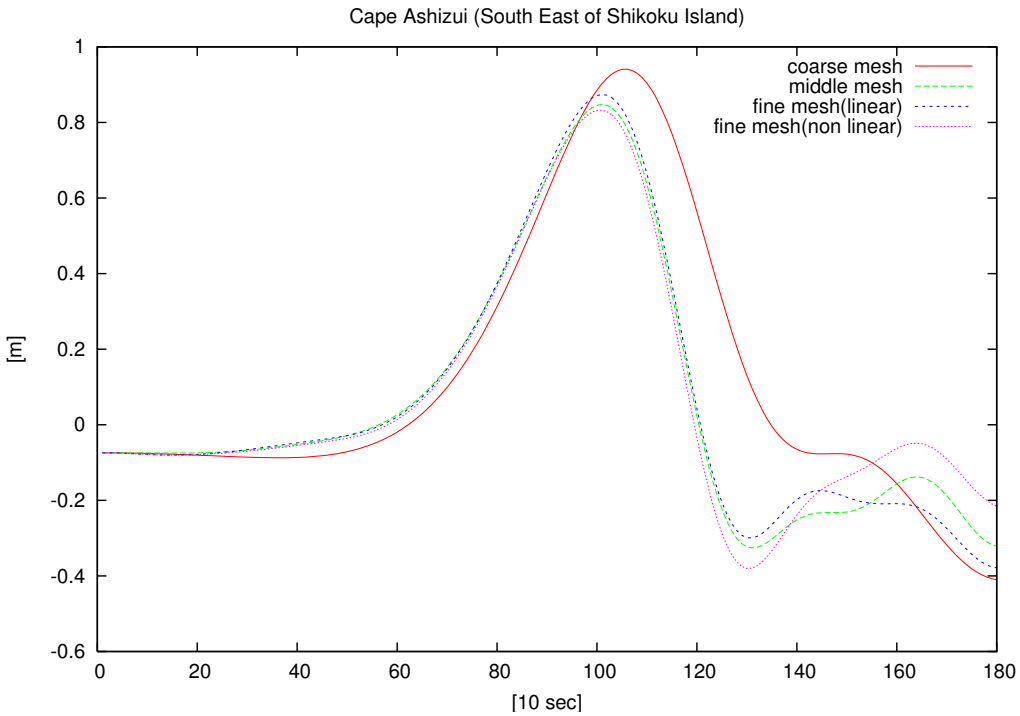

Figure 9: Cape Ashizuri.

and so on. We approximate the partial derivatives on the right-hand side of equation (11) in a similar way to $\partial\zeta/\partial x$ in (9).

6 Numerical results

Figure 9 shows the numerical results based on several mesh refinements at Cape Ashizuri and Figure 10 shows the comparison of the wave height at Cape Ashizuri and a point of Cape Ashizuri Offing. The supplementary movie

Table 2: Comparison of wave height at the offing and the coast

area	maximum of wave height(m)		sea depth(m)			estimated height(m)	
	H_o	H_c[A]	h_o	h_c	$(h_o/h_c)^{1/4}$	H_c[B]	[A]/[B]
Ashizuri	0.6036	0.8326	401.4	92.0	1.4453	0.8723	95.4%
Muroto	0.7552	0.9730	167.3	47.0	1.3736	1.0373	93.8%
Hiwasa	0.8101	1.4358	408.1	66.0	1.5769	1.2774	112.4%
Inami	0.9550	1.4178	209.2	56.0	1.3903	1.3277	106.8%

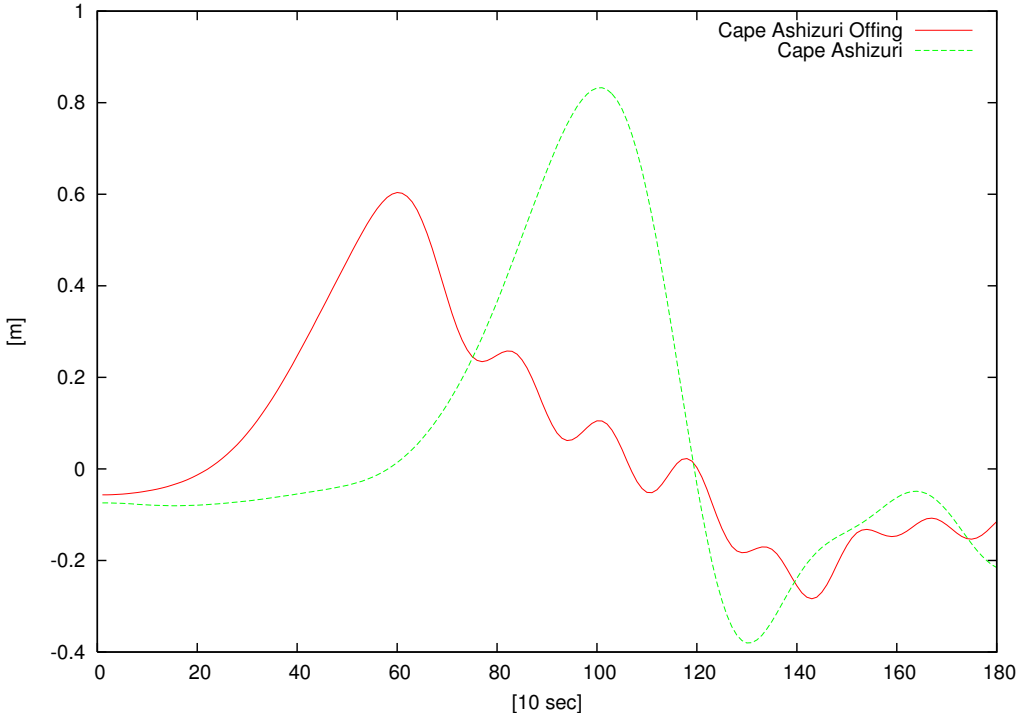

Figure 10: Cape Ashizuri and Cape Ashizuri Offing

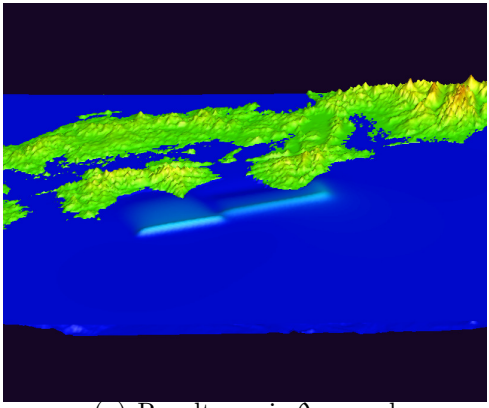

(a) Result movie 0 second

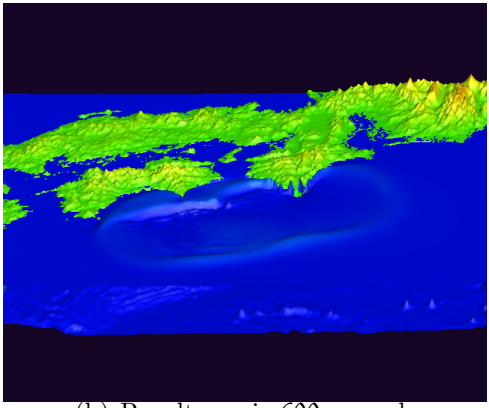

(b) Result movie 600 seconds

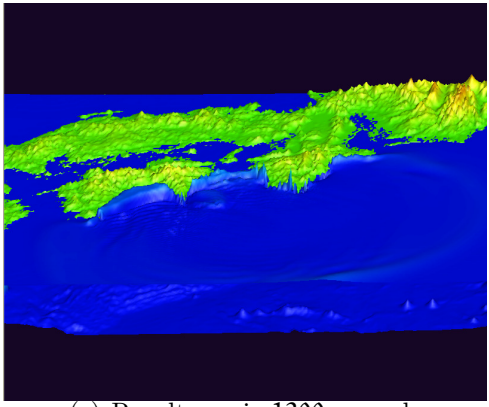

(c) Result movie 1200 seconds

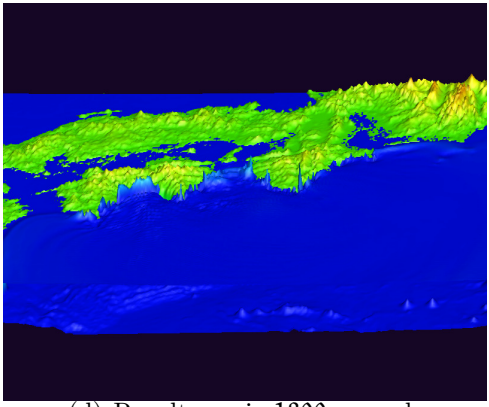

(d) Result movie 1800 seconds

Figure 11: result movie.

file.mpg[1] shows the wave motion resulting from the numerical simulation; Figures 11(a)–11(d) shows snapshots at every 600 seconds. Figure 11(a) shows the initial surface displacement. Figure 11(b) shows that the tsunami reaches the coast of Kii Peninsula ten minutes after the initial surface displacement. Figure 11(c) shows that the tsunami arrives at the Pacific coast of Shikoku Island twenty minutes after the initial surface displacement. The delay of the arrival is caused by the shallow sea area which covers the Pacific side of the island. Figure 11(d) shows that it takes thirty minutes for the tsunami to reach the coast of Tokai district. Wave heights at various points are summarized in Table 2. The maximum wave height at the coast is observed about 600 seconds after the maximum wave height is observed at the 20 km offing from the coast.

Green's law shows that the wave height at the coast, H_c, is estimated by

$$H_c = H_o \left(\frac{h_o}{h_c} \right)^{1/4},$$

where the H_o is the wave height of the offing, h_o represents the sea depth of the offing, and h_c denotes the sea depth of coast [7]. The result of this simulation shows that the calculated maximum wave heights at the four coasts are within the limits of 93.8% to 112.4% of the heights estimated using Green's law.

7 Conclusion

The wave heights at the coast in this simulation correspond well to those estimated by Green's law. More important is the agreement between the simulated and observed data. We can get historical data about tides at many tidal stations provided by Ministry of Land or Meteorological Agency in Japan. But most of the tidal stations are located at irregular locations along

[1] http://journal.austms.org.au/ojs/index.php/ANZIAMJ/article/downloadSuppFile/3969/722

the coastline, or at deep places in bays. Precise simulation of a tsunami requires local mesh refinement.

Acknowledgements The depth data of the sea are based on the charts produced by the Japan Hydrographic Association, Marine Information Research Center MIRC-JTOPO30 M1406 2006/09/11 Ver. 1.0.1.

References

[1] I. Aida. Numerical experiments for the tsunamis generated off the coast of the Nankaido district. *Bull. Earthquake Research Institute*, 56:713–730, 1981. C1038

[2] J. D. Lambert. *Computational Methods in Ordinary Differential Equations*. John Wiley & Sons, Chichester, 1973. C1042

[3] L. Mansinha and D. E. Smylie. The displacement fields of inclined faults. *Bulletin of the Seismological Society of America*, 61(5):1433–1440, October 1971. C1035

[4] A. R. Mitchell and R. Wait. *The Finite Element Method in Partial Differential Equations*. John Wiley & Sons, Chichester, 1977. C1042

[5] Geospatial Information Authority of JAPAN. The Niigata–Kobe tectonic zone. http://cais.gsi.go.jp/Virtual_GSI/Tectonics/Niigata_Kobe/niigata_kobe.html, January 14, 2011. C1032

[6] T. Okamoto, M. Kawahara, N. Ioki, and H. Nagaoka. Two-dimensional wave run-up analysis by selective lumping finite element method. *International Journal for Numerical Methods in Fluids*, 14(1992):1219–1243, 1992. C1042

[7] N. Shuto, F. Imamura, S. Koshimura, K. Satake, and H. Matsutomi. *Encyclopedia of Tsunami*. Asakura Shoten, 2007 (in Japanese). C1046

Author addresses

1. **Y. Otani**, Graduate School of Environmental Science, Okayama University, Okayama 700-8530, Japan.
mailto:gev421104@s.okayama-u.ac.jp
2. **K. Yamamoto**, Graduate School of Environmental Science, Okayama University, Okayama 700-8530, Japan.
3. **Hashentuya**, Graduate School of Environmental Science, Okayama University, Okayama 700-8530, Japan.
4. **M. Watanabe**, Graduate School of Environmental Science, Okayama University, Okayama 700-8530, Japan.
mailto:watanabe@env.okayama-u.ac.jp